ISA Transactions 64 (2016) 384–393

Contents lists available at ScienceDirect

ISA Transactions

journal homepage: www.elsevier.com/locate/isatrans

freepaper.me FREE paper

Design and experimental analysis of an advanced static VAR compensator with computer aided control

Erdal Irmak [a,*], Ramazan Bayındır [a], Ali Köse [b]

[a] Gazi University, Faculty of Technology, Electrical and Electronics Engineering Department, Ankara, Turkey
[b] Gazi University, Technical Sciences Vocational Colleague, Ankara, Turkey

ARTICLE INFO

Article history:
Received 21 February 2016
Received in revised form
21 April 2016
Accepted 11 May 2016
Available online 24 May 2016
This paper was recommended for publication by Dr. Jeff Pieper

Keywords:
Reactive power compensation
Fixed capacitor-thyristor controlled reactor
Energy monitoring and control

ABSTRACT

This study presents integration of a real-time energy monitoring and control system with an advanced reactive power compensation unit based on fixed capacitor-thyristor controlled reactor (FC-TCR). Firing angles of the thyristors located in the FC-TCR are controlled by a microcontroller in order to keep the power factor within the limits. Electrical parameters of the system are measured by specially designed circuits and simultaneously transferred to the computer via a data acquisition board. Thus, real time data of the system can be observed through a visual user interface. The data obtained is not only analyzed for control process, but also regularly saved into a database. The system has been tested in laboratory conditions under different load characteristics and experimental results verified that the system successfully and accurately achieves compensation process against the all operational conditions.

© 2016 ISA. Published by Elsevier Ltd. All rights reserved.

1. Introduction

The energy quality is an important issue nowadays and it depends on continuity of energy, fixed grid frequency, constant and sinusoidal supply voltage, value of the power factor, balance of phase voltages and currents, and the harmonic distortions [1–3]. Among these criteria, power quality is of great importance and can be improved with compensation of reactive power. Due to usage of loads with low power factors in industry and the increase of nonlinear devices in power systems, energy generation and distribution companies have to produce additional reactive energy and to transfer it over transmission lines with high losses. Therefore, improving the power factor is a mandatory operation for all industrial enterprises in order to minimize the costs, and to provide the energy efficiency.

Reactive power compensation is defined as the management of reactive power to improve the performance of alternating-current (AC) power systems. In general, the problem of reactive power compensation is related to load and voltage support. In load support, the objectives are to increase the value of the system power factor, to balance the real power drawn from the AC supply, to enhance voltage regulation, and to eliminate current harmonic components. Voltage support is generally required to reduce voltage fluctuation at a given terminal of a transmission line. Reactive power compensation in transmission systems also improves the stability of the AC system by increasing the maximum active power that can be transmitted [4]. The reactive power drawn by non-compensated loads causes the voltage changes in a finite non-zero impedance grid. Operating the compensation structures on the load side is a practical solution way to reduce these changes [5–7].

Traditionally, the power factor correction process has been typically achieved by capacitor banks, synchronous motors, microcontroller based reactive power relays [5–9]. However, these conventional methods are usually inadequate for the loads that have high power and short transition times between turn-on and turn-off operations. For this reason, static VAR compensators (SVC) have been developed. SVCs adjust the susceptance in each phase by controlling the firing angles of the thyristor controlled reactor [10]. The SVC can be found in applications such as power line compensation, compensation of railway feeding system, reducing disturbance from rolling mills and arc furnace compensation [11].

Energy monitoring is another crucial subject for power systems. In the recent literature, different methods and various interface options are recommended for monitoring of energy consumed in industrial enterprises, buildings, schools and shopping centers [12–19]. Among several methods, computer based measuring and monitoring systems have been gained popularity [20–22]. A common solution in energy tracking and monitoring systems is to employ an energy analyzer. Measured electrical

* Corresponding author. Tel.: +90 312 202 85 52.
E-mail addresses: erdal@gazi.edu.tr (E. Irmak), bayindir@gazi.edu.tr (R. Bayındır), alikose@gazi.edu.tr (A. Köse).

http://dx.doi.org/10.1016/j.isatra.2016.05.005
0019-0578/© 2016 ISA. Published by Elsevier Ltd. All rights reserved.

parameters can be seen on the analyzer screen or can be monitored from a computer using the communication port of analyzer. Moreover, the measured results are likely to be observed over the internet using GPRS, Modbus and TCP/IP protocols by using new generation energy analyzers. However, achieving the energy monitoring and power factor correction processes through a data acquisition (DAQ) board has not been sufficiently studied yet.

In this context, commercial ready-to-use energy analyzers has been not used in this study as a difference from similar ones in the recent literature. For this aim, special circuits have been designed which measure the required signals quickly. Thus, cost of the system is considerably reduced. Furthermore, the switching devices are triggered accurately without any delay in each alternance because of using dsPIC microcontroller which is capable of operating higher frequencies than similar microcontrollers. Thus, speed and accuracy of the system has been increased. Moreover, electrical parameters of the power system are measured continuously and transferred to the computer in real time via a Data Acquisition (DAQ) board. Accordingly, it is possible to monitor all system data in real time through a visual interface. The system designed has been tested under different types of loads and experimental results show that it has considerably quite response time and high accuracy as well.

2. Theoretical background of FC-TCR

Thyristor controlled SVC systems are combination of a thyristor controlled reactor with a fixed capacitor bank and can be classified as following [6,23,24]:

- Thyristor switched capacitor (TSC).
- Thyristor switched reactor (TSR).
- Thyristor switched capacitor-Thyristor controlled reactor (TSC-TCR).
- Fixed capacitor-Thyristor controlled reactor (FC-TCR).

Among these methods, this study focuses on the last one called as FC-TCR. The equivalent circuit of a FC-TCR is shown in Fig. 1(a). As seen on figure, the capacitor draws a constant current from the source (V_S). The reactive current (I_S) drawn from the source is controlled by adjusting the firing angles of thyristors (T_1 and T_2) which are connected in series to the reactor (L). FC-TCR can provide continuous lagging and leading VARs to the system. Leading VAR is supplied by the capacitor. For supplying lagging VAR, TCR is generally rated larger than the capacitor. While fixed capacitor produces reactive power, thyristor controlled reactor consumes it. The control characteristics of SVC is shown in Fig. 1(b) where ADB line points out the control range.

The SVC control range is described by

$$V_s = V_{ref} + X_s.I_s \tag{1}$$

where X_s is the inclination of the control characteristic line [27]. V_{ref} is the SVC voltage when $I_S=0$.

The first step of SVC design process is the determination of the capacitor value. For this aim, the capacitive reactive power demand required for minimizing the voltage is calculated assuming the system operates as uncompensated. The result obtained determines the maximum capacitive power of SVC. Then, inductive reactance of TCR is determined depending on the rate of inductive and capacitive operating range. Using Kirchhoff equations, the value of the fixed capacitor and the value of the reactor are calculated with Eqs. (2) and (3):

$$V_s = \frac{(I.\ \sin\ \varphi)\max}{\omega.C} \tag{2}$$

$$V_s = \left[(I.\ \sin\ \varphi)\max - (I.\ \sin\ \varphi)\min\right].\omega.L \tag{3}$$

where V_s refers to the voltage applied, C refers to the capacity, L refers to the inductance, I refers to the circuit current, ω refers to the angular frequency of voltage. $(I.\sin\phi)_{\max}$ and $(I.\sin\phi)_{\min}$ indicate the maximum and the minimum values of lagging reactive currents, respectively. The current in TCR can be controlled by adjusting the firing angle (α) and its instantaneous value over half a cycle (i_{TCR}) is given by Eq. (4) [25]:

$$i_{TCR}\left\{\begin{array}{ll} = \frac{\sqrt{2}.V_s}{\omega.L}(\cos\ \alpha - \cos\ \omega t), & \alpha < \omega t < \alpha+\sigma \\ = 0, & \alpha+\sigma < \omega t < \alpha+\pi \end{array}\right\} \tag{4}$$

Similarly, the reactive power in the TCR is calculated by using Eq. (5) [26]:

$$\theta_{TCR} = \frac{V_s^2}{\pi.\omega.L}(2\pi - 2\alpha + \sin\ 2\alpha) \tag{5}$$

The current waveform of a one-phase TCR is shown in Fig. 1(c). As seen, the current is non-sinusoidal and contains harmonics which are functions of the conduction angle (σ). The fundamental component of the TCR current (I_1) is given by [25]:

$$I_1 = B_{TCR}(\sigma).V \tag{6}$$

$$B_{TCR} = \frac{\sigma - \sin\ \sigma}{\pi.\omega.L} \tag{7}$$

The conduction angle σ is related to α as seen in Eq. (8).

$$\sigma = 2(\pi - \alpha) \tag{8}$$

All the equations and descriptions given above show that the power factor can be corrected continuously by adjusting the reactor current with the help of controlling thyristors. Thanks to using this method, compensators provide rapid response to the need of reactive power but produce discontinuous current waves and single-level discrete harmonic currents as a result of firing

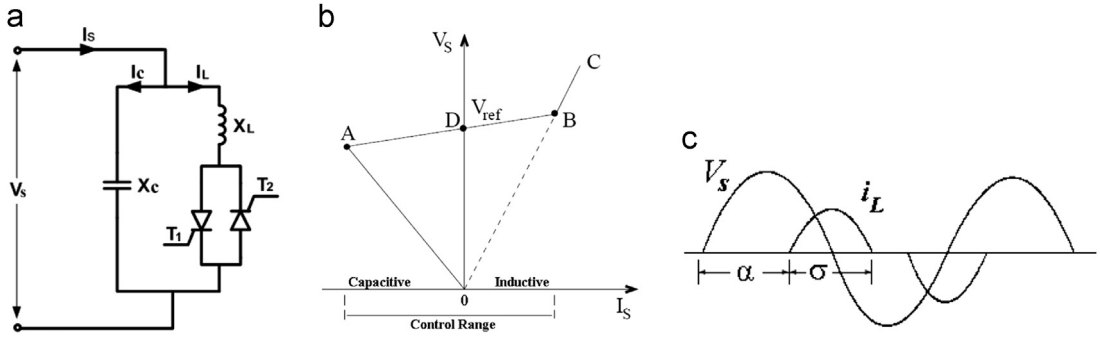

Fig. 1. (a) Simple power system model of FC-TCR. (b) Control characteristics of SVC. (c) Waveforms of V_S and I_L.

freepaper.me FREE paper

angle control. For this reason, the fixed capacitor is used in order to eliminate the low-level harmonics. If the two thyristors are fired symmetrically in positive and negative half-cycles, then odd-order harmonics are only produced. These harmonics can be figured out through a Fourier analysis of higher-frequency components. The RMS value of the current harmonics are calculated as a function of the firing angle using Eq. (9) [27].

$$I_{Ln}(\alpha) = \frac{V}{\omega L}\cdot\frac{4}{\pi}\cdot\left(\frac{\sin\ \alpha.\ \cos(n\alpha) - n.\ \cos\ \alpha.\ \sin(n\alpha)}{n(n^2-1)}\right) \quad (9)$$

In Eq. (9), n can be calculated with the formula of $n=2k+1$, where k indicates the standard harmonic orders like 1, 2, 3, and so on.

3. System design

In the study, electrical parameters of a power system consisting of resistive and inductive loads are measured firstly and then transferred to the dsPIC microcontroller in order to detect the power factor. Once the power factor is defined, the system automatically calculates the required reactive power that will be supplied by the reactor. Finally, thyristors are triggered according to the reactive power calculation. Since the system includes a computer interface, a powerful data acquisition board is used to transfer the data between the computer and the hardware units. A general block diagram of the system is shown in Fig. 2.

3.1. Controller Unit

In the presented study, a dsPIC microcontroller is used to trigger the thyristors. dsPIC is an efficient controller with its less cost and high resolution as compared to similar ones such as PIC, PLC, DAQs and DSP. Powerful features of the controller are made it easy to trigger the thyristors accurately and to measure the power factor quickly. To detect the power factor, external interrupt channels are used to capture the time difference between the current and the voltage signals. Two PWM channels are used to trigger the thyristors. Hi-Tech C language is used to develop the software embedded into dsPIC, flowchart of which is given in Fig. 3.

As seen in Fig. 3., the dsPIC first receives the zero crossing points of the current signal and then the same points of the voltage signal. A timer starts to count when the current signal is received and stops counting as soon as the voltage signal is received. Thus, the time difference between the voltage signal and current signal is obtained. By using the grid frequency, the time of a voltage period can be calculated easily ($T=1/f$); e.g., if the frequency is 50 Hz, the time period of the voltage will be 20 ms. As a simple proportion, if a sinusoidal signal completes its cycle (from 0° to 360°) in 20 ms, each 1 ms corresponds to 18° as electrical angle. By using this approach, the time difference measured by the microcontroller can be easily used to calculate the power factor value. For instance, assuming the time difference is measured as 2 ms, this means the angle between the current and the voltage is about $2\times 18=36°$, and thus the power factor value will be cos $36°=0.809$ for this operating scenario.

Once the power factor value is calculated as mentioned above, it is compared to the reference value and the required firing angles are determined considering to this comparison. All these processes are automatically executed by the microcontroller in accordance with the mathematical rules given in Section 2.

3.2. Design of current and voltage measurement circuit

Since the input channels of microcontroller can only accept the signals in the range of 0–5 V, an integrated current and voltage measurement card is designed as shown in Fig. 4. The grid voltage signal is measured from the card inputs indicated as number 1 on the figure. This measured voltage is firstly reduced to lower level (*0–5 V*) by the transformer and then applied to the first input channel of zero crossing circuit. As seen on the left bottom side of card (indicated as number 5), LEM CAS 25-NP current sensor is connected in series with the load to obtain the current information. Similar to the voltage measurement operation, the current sensor generates a low level (0–5 V) output signal depending on the load current and this output signal is applied to the second input channel of zero crossing circuit.

The designed measurement card not only measures the voltage and current signals but also supplies power to all other circuits on the experimental set. For example, the driver circuits of thyristors are fed

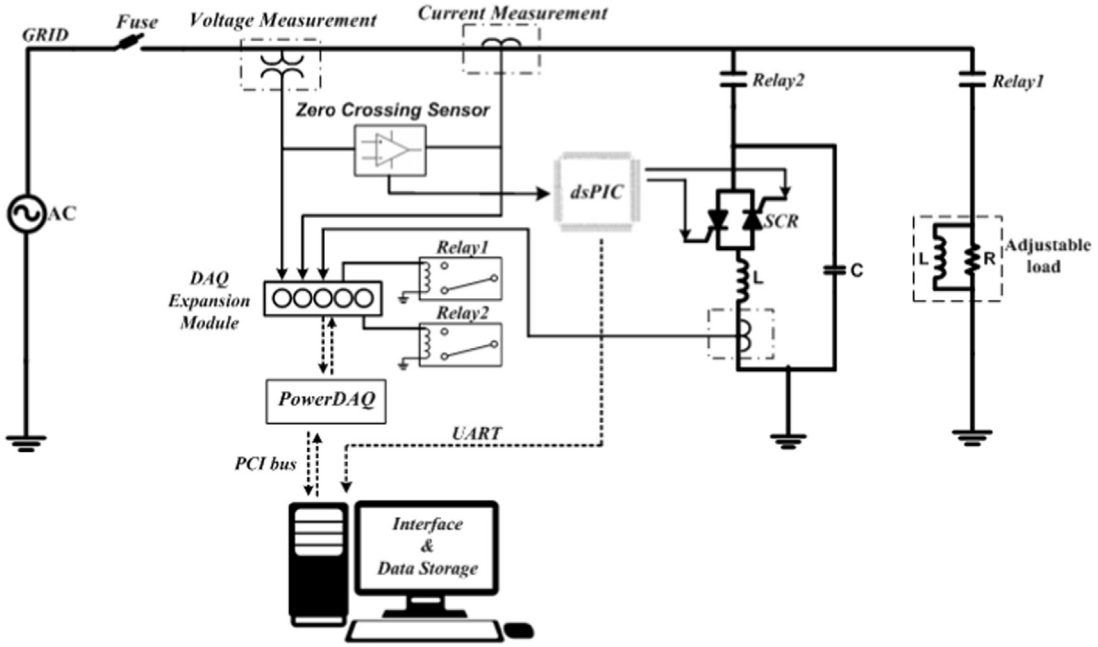

Fig. 2. The block diagram of the power factor correction system.

freepaper.me FREE paper

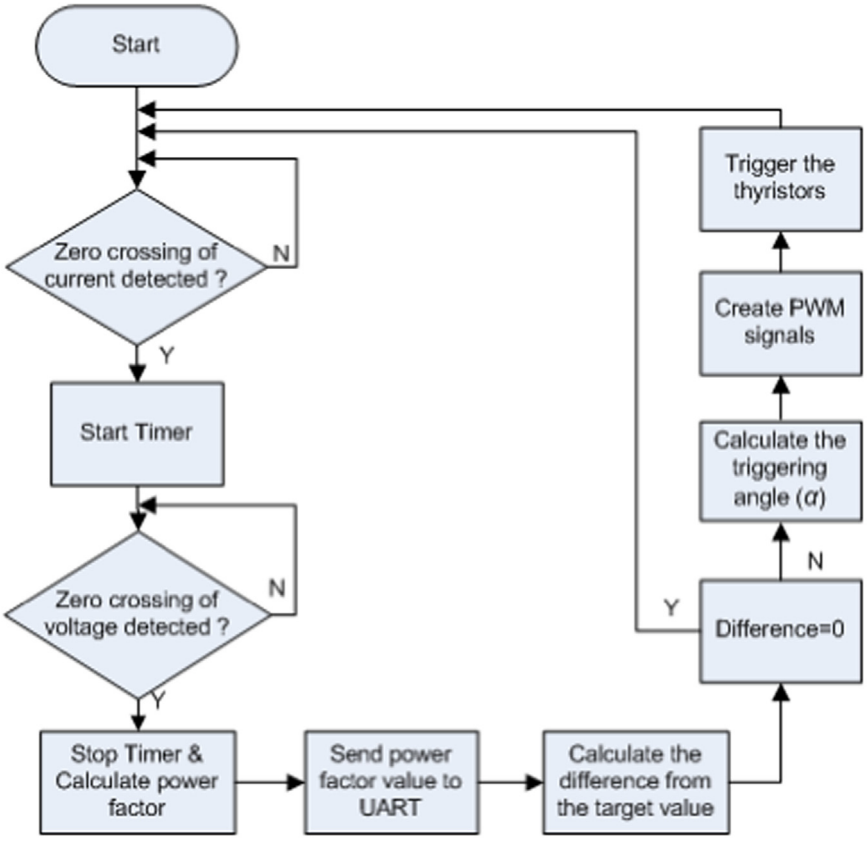

Fig. 3. Flowchart of the software embedded into the microcontroller.

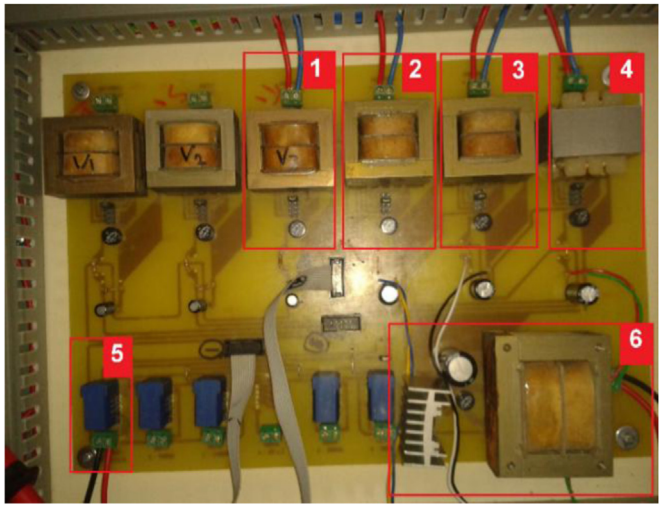

Fig. 4. Current–voltage measurement card.

from the number 2 and the number 3, the relays used for on/off control of loads are fed from the number 4, and the own power demand of the measurement card is supplied from the number 6. Thus, the system does not require to any external power supply.

3.3. Zero crossing detector

The term "zero-crossing" indicates a special point where the sign of a mathematical function changes (e.g. from positive to negative), represented by a crossing of the axis (zero value) in the graph of the function [28]. Accordingly, a zero crossing detector has been used in this study to detect the time difference between the current and the voltage signals at the moment both of them are crossing over the zero. The view of zero-crossing detector developed is given in Fig. 5(a). As seen on the figure, the voltage and the current signals are connected to the input channels of the detector. A square wave signal is generated at the output of the detector during the positive period of input signal. Fig. 5(b) shows a sample output signal which verifies the zero-crossing point is detected successfully.

3.4. Optically isolated relay circuit

Since the digital I/O channels of DAQ board process to low level signals (about 5 V) and it is not possible to drive the devices operating with higher voltages, a special driver circuit is designed in the study for performing the on/off controls of the compensator and the loads which have 220 V operating voltage. For this aim, some relays are used in the driver circuit. Because these relays can be activated by low level signals, it has been possible to control them through the digital output signals of the DAQ board. Furthermore, the switching contacts of the relays can drive higher voltage devices (about 250 V). Thus, the loads and the compensator are controlled easily from the DAQ board by using the driver circuit. A view of the circuit is shown in Fig. 6. As seen on the figure, the power layer (operating at 220 V voltage level) and the control layer (operating with 5 V control signals) are isolated from each other using 4N25 opto-couplers in order to protect the DAQ board against the possible electrical faults.

3.5. Thyristor driver circuit and FC-TCR design

A FC-TCR circuit is designed in the study which automatically adjusts the firing angles of the thyristors. A simplified electrical model of the designed single phase FC-TCR type compensator is shown in Fig. 7.

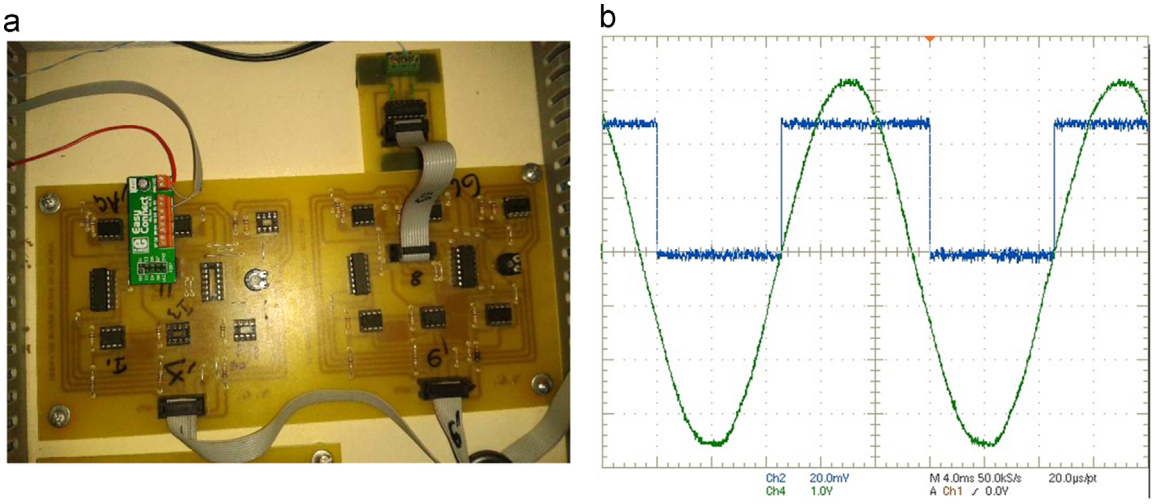

Fig. 5. (a) A view of the zero crossing detector designed. (b) Output signal of the detector.

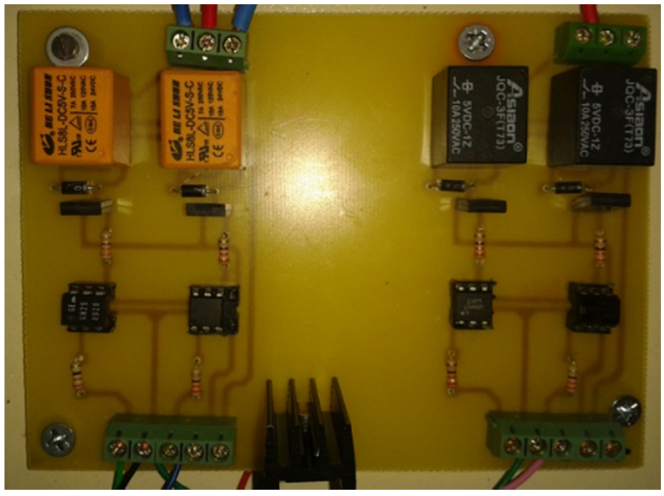

Fig. 6. Isolated relay card.

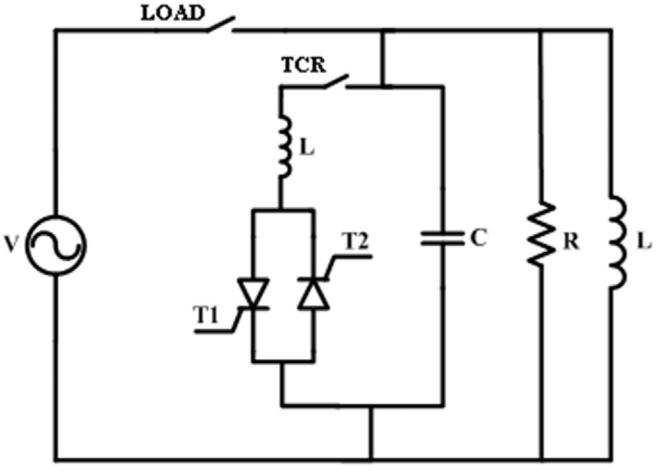

Fig. 7. Equivalent circuit of FC-TCR compensator.

Since the triggering signals sent from the microcontroller cannot be applied directly to the thyristors, 4N25 series optocouplers are used for isolation purposes and IRF530 series MOSFETs are used for switching. In the experimental set, CLA50E1200HB series high-impact thyristors are preferred that can operate under 1200 V, 50 A. A view of the designed driver circuit and thyristors are shown in Fig. 8(a) and (b).

As the final step, all hardware components described separately above are integrated on a circuit platform to obtain a multi-functional experimental set, the appearance of which is shown in Fig. 9. The components installed on the set are defined below by referring the capital letters on the figure.

A: The current–voltage measurement card.
B: The second current measurement card using LEM HAL 50-S current sensors.
C: Relays for activating the load and the compensation system.
D: Zero crossing detection circuit.
E: Integrated circuit for true-RMS measurements.
F: Insulated relay board.
G: Driver circuit for thyristors.
H: Thyristors with cooling materials.

4. Experimental study

In order to test and to verify the presented system, an experimental setup is built in laboratory conditions. The appearance of the setup is shown in Fig. 10. Referring the numbers on the figure, the experimental setup consists of a control computer indicated as 1, measurement and control cards indicated as 2, a scope indicated as 3, data acquisition board and microcontroller unit indicated as 4 and loads indicated as 5.

For experimental tests, adjustable loads are used in the study as shown in the part 5 of Fig. 10. Each load group is consisted of three equal branches. Thus, while the L_1 branch of the inductive load group is used as inductive load for the power system, the L_2 branch is used as the reactor. On the other hand, the L_3 branch is connected in serial to the capacitor as a reactor for filtering purposes. Similarly, the R_1 branch of the resistive group is used as resistive load for the power system and the C_1 branch of the capacitive load group is connected in parallel to the system to act as the fixed capacitor. Resistance (R), inductance (L), capacitance (C), inductive reactance (X_L) and capacitive reactance (X_C) values of the loads in each step are manually measured before the experimental study and given in Table 1.

As mentioned before, the study includes not only a compensation system but also a user friendly energy monitoring and control interface. A screenshot of the developed interface is given

freepaper.me FREE paper

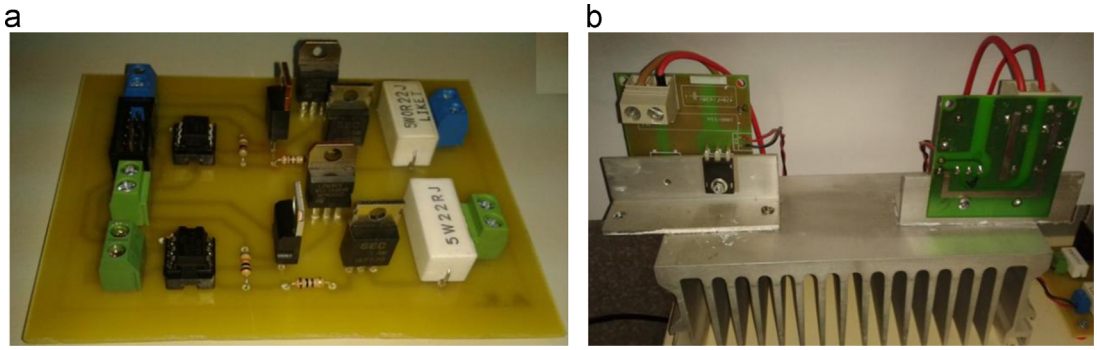

Fig. 8. (a) Thyristor driver circuit. (b) Symmetrically connected thyristors.

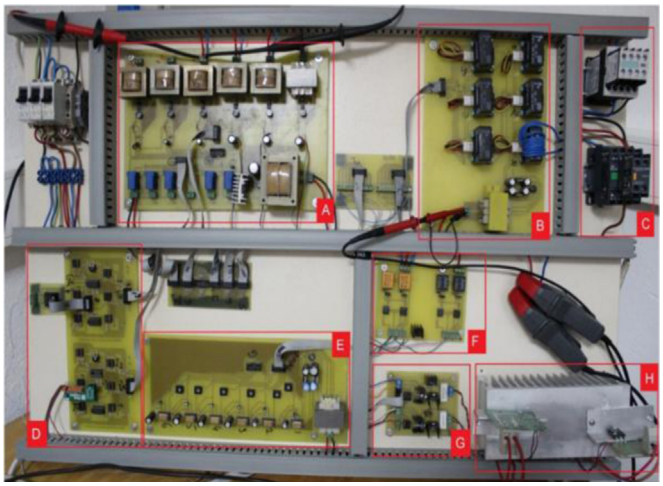

Fig. 9. Experimental set designed.

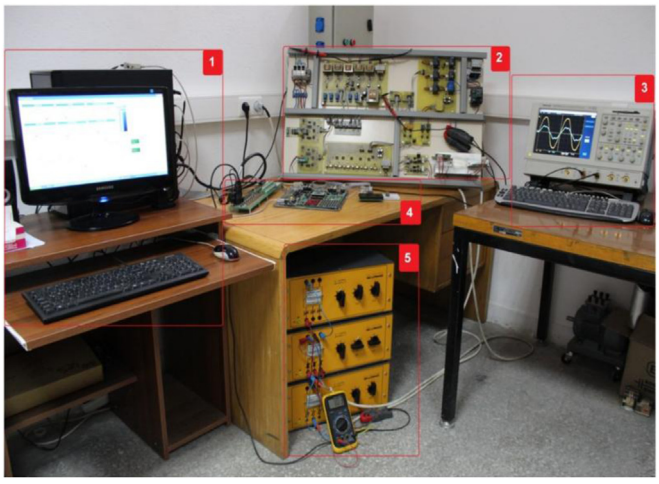

Fig. 10. The appearance of the experimental set.

in Fig. 11. Referring the numbers on the figure, all electrical parameters of the system are monitored at the part 1. The Load On/Off and the TCR On/Off control buttons are located in the part 2. The working ratio of TCR after the compensation is activated is shown in part 3 visually by using a tank indicator. Finally, voltage, current and reactor current graphics are presented in part 4.

4.1. Experimental results

The first experimental test is conducted for uncompensated operation. For this purpose, the load is adjusted to 329 Ω resistive value, 966 Ω inductive reactance value (3.07 H) and 227 Ω (14.02 μF) capacitive reactance value for the fixed capacitor. Then, the system is activated to supply the load by clicking on the Load On/Off button on the visual interface.

Table 1
Load values in each level.

Step	R (Ω)	L (H)	X_L (Ω)	C (μF)	X_C (Ω)
1	1048	4.25	1337	2.16	1474
2	766	3.07	966	3.09	1030
3	329	2.68	843	5.21	610
4	295	1.78	562	8.27	385
5	257	0.94	295	10.47	304
6	139	0.85	267	14.02	227
7	124	0.51	163	18.83	169

In order to verify the graphics monitored on the interface, a scope is connected to the experimental set externally and then the real time graphic measured by the scope is compared to the graphical result seen on the visual interface. While Fig. 12 (a) illustrates the view of interface during the uncompensated operation, Fig. 12(b) presents the scope results captured simultaneously under the same conditions. Comparison of both figures verifies that the system developed successfully measures and accurately monitors all parameters. It should be noted that all data used for plotting on the interface is multiplied by 100 for a better analysis of the current graphics. As it can be seen on Fig. 12, the current signal is forward from the voltage signal and the power factor is measured as 0.669 leading because of the of fixed capacitor. For this experimental test, the active and the reactive power values are measured as 162.51 W and 180.49 VAr, respectively.

After the uncompensated test of the system, the compensation process is activated by clicking on the TCR On/Off button on the interface. As previously mentioned, the microcontroller continuously detects the power factor as long as the system is being operated and immediately calculates the required triggering angle for the thyristor. Fig. 13(a) and (b) illustrates the view of interface and the scope result respectively after the TCR is activated. As seen from both figures, while the reactive power drawn from the grid is reduced, the current value is increased; hence, there is a slight increase in the active and apparent power values because the reactor is turned on. It is also seen from the upper right side of the interface that the system uses the 92.5% of total power of reactor by automatically adjusting the switching ratio of the thyristor in order to compensate the capacitive effect and to improve the power factor. As a result of this process, the phase angle between the current and the voltage is decreased to 3 degrees and the power factor is improved to 0.998 lagging.

For the second experimental test, values of the parallel RLC load are manually changed to 257 Ω resistive load, 267 Ω inductive reactance (0.85 H) and 227 Ω (14.02 μF) capacitive reactance for

freepaper.me FREE paper دانلود کننده مقالات علمی

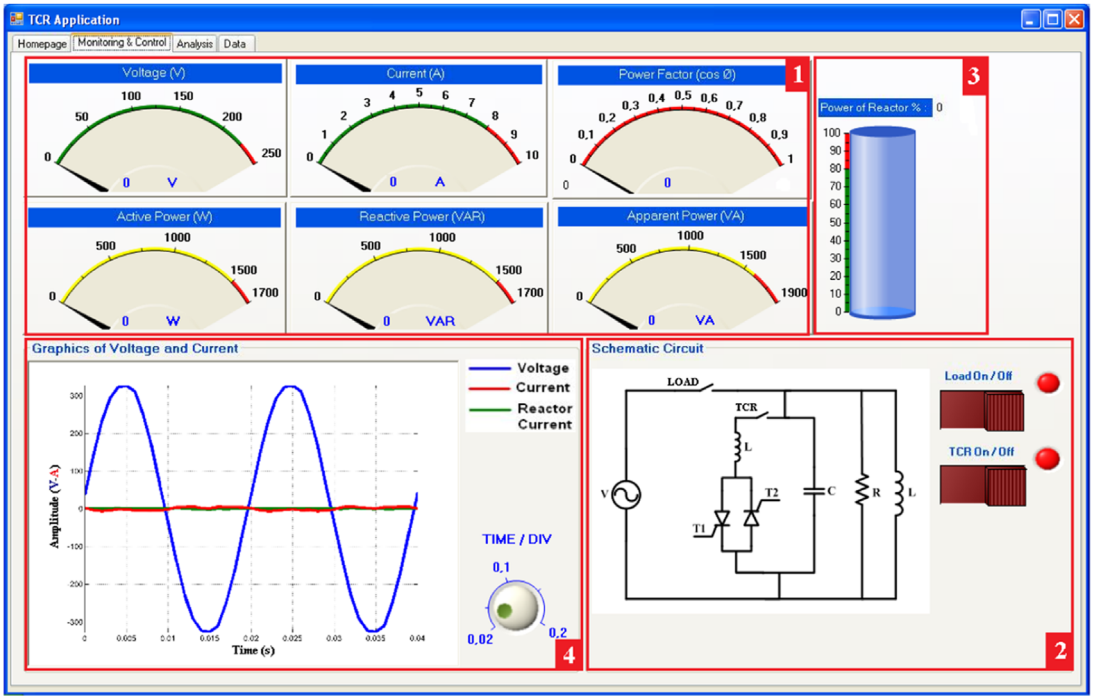

Fig. 11. Monitoring and control interface screen.

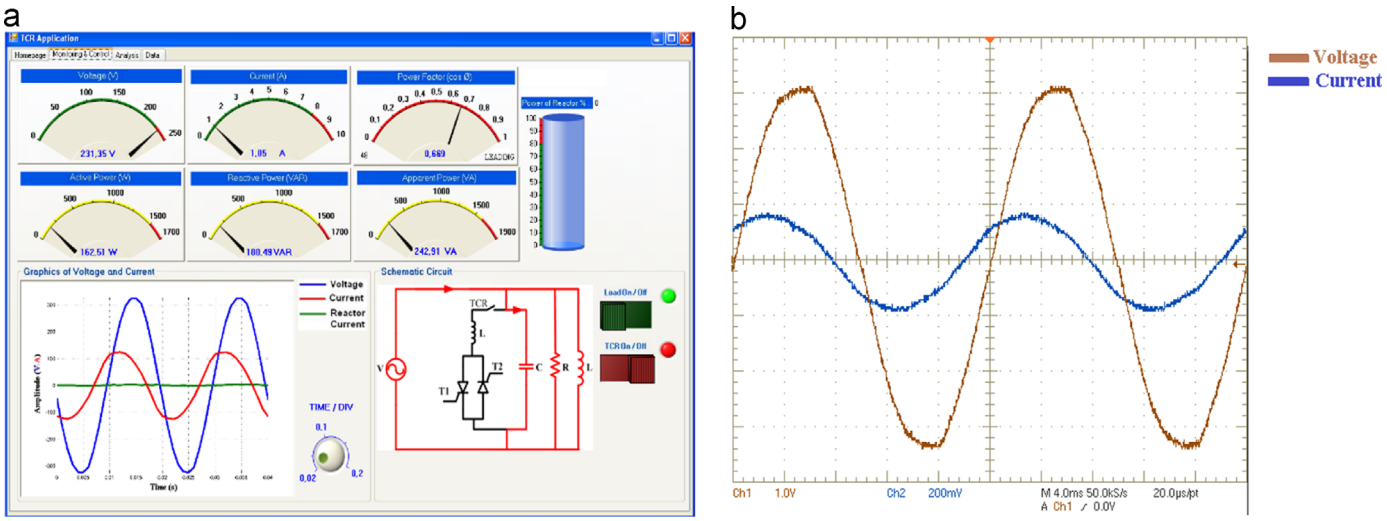

Fig. 12. (a) The view of interface before compensation ($R=329\ \Omega$, $L=3.07$ H, $C=14.02\ \mu$F). (b) Real time scope results for the same operational conditions.

the fixed capacitor. Then, the system is tested against these load conditions. For this aim, the TCR is turned off at first (uncompensated test) and results obtained are given in Fig. 14(a) and (b). As seen from both figures, the current is about 0.92 A and the voltage is about 232.23 V. The power factor is measured as 0.981 leading due to the fixed capacitors. Since the TCR is not turned on yet, the tank indicator on the screen seems empty (0%).

After the uncompensated test is completed, the TCR is turned on to start the compensation process and then the system response against this change is experimentally analyzed. Fig. 15(a) and (b) presents the results of compensated test. As seen from both figures, the power factor is successfully improved to 0.99 lagging as soon as the TCR is started to operation. Because the inductive reactive power value of the load is higher than the previous experiment, triggering rate of the thyristor is reduced. Therefore; to compensate the capacitive effect, the system is just used the 45.8% of the reactor power as seen on the tank indicator on Fig. 15(a).

In order to test the accuracy and performance of the system under several loading conditions, another experimental study is conducted by decreasing the resistive value of the load to 139 Ω and increasing its inductive value to 562 Ω (1.78 H). Similar to the previous experiments, the system is firstly activated while the TCR is off and the results obtained in this case are presented in Fig. 16(a) and (b). Considering to the previous tests, the RMS value of the current drawn from the grid is increased to 1.77 A in this situation due to the decrease on the impedance. The power factor is measured as 0.939 leading because of the effect of capacitor. As a result of higher load current, active, reactive and apparent power values are also increased.

Once the system response is investigated for uncompensated operation, the TCR is turned on by clicking on the TCR on/off button on the interface. The view of the interface and the real time scope results after activating the compensation process are given in Fig. 17(a) and (b), respectively. As compared to Figs. 16 and 17, it

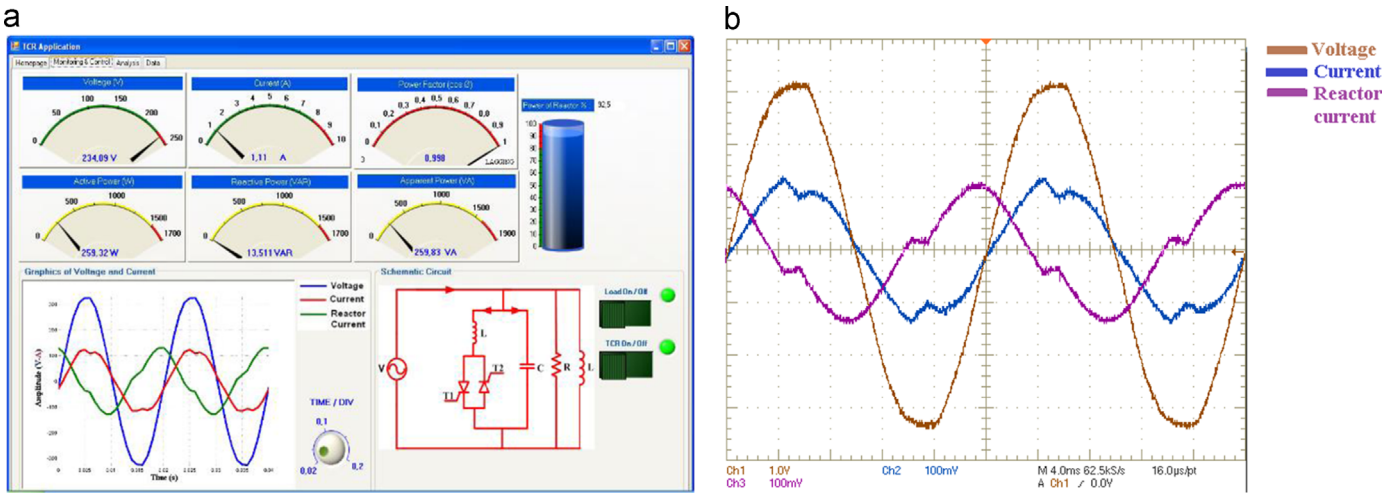

Fig. 13. (a) The view of interface after compensation ($R=329\ \Omega$, $L=3.07$ H, $C=14.02\ \mu$F). (b) Real time scope results for the same operational conditions.

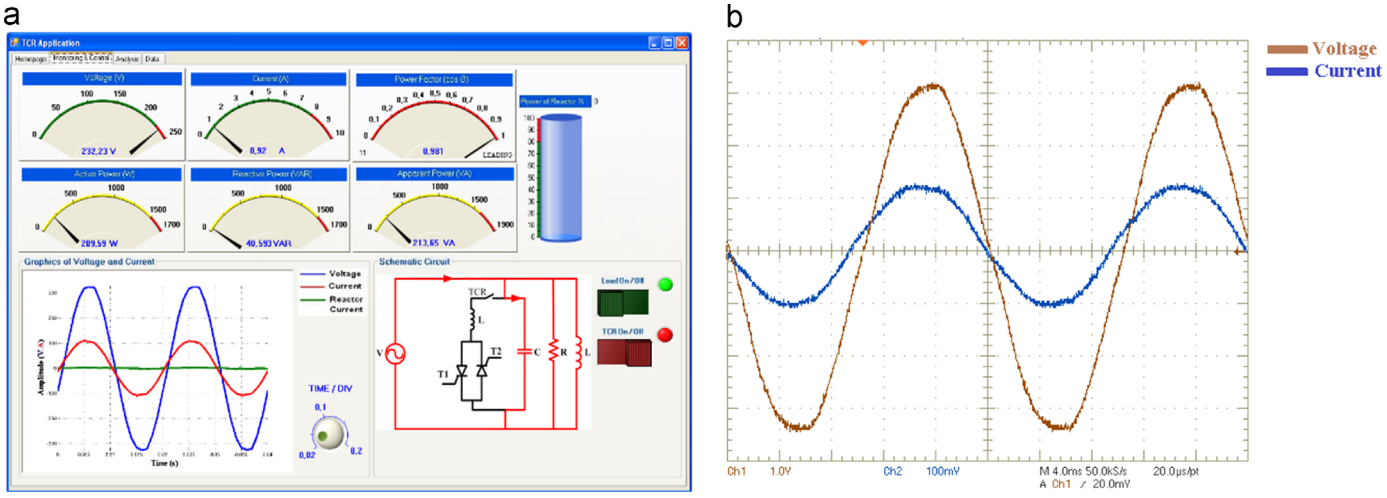

Fig. 14. (a) The view of interface before compensation ($R=257\ \Omega$, $L=0.85$ H, $C=14.02\ \mu$F). (b) Real time scope results for the same operational conditions.

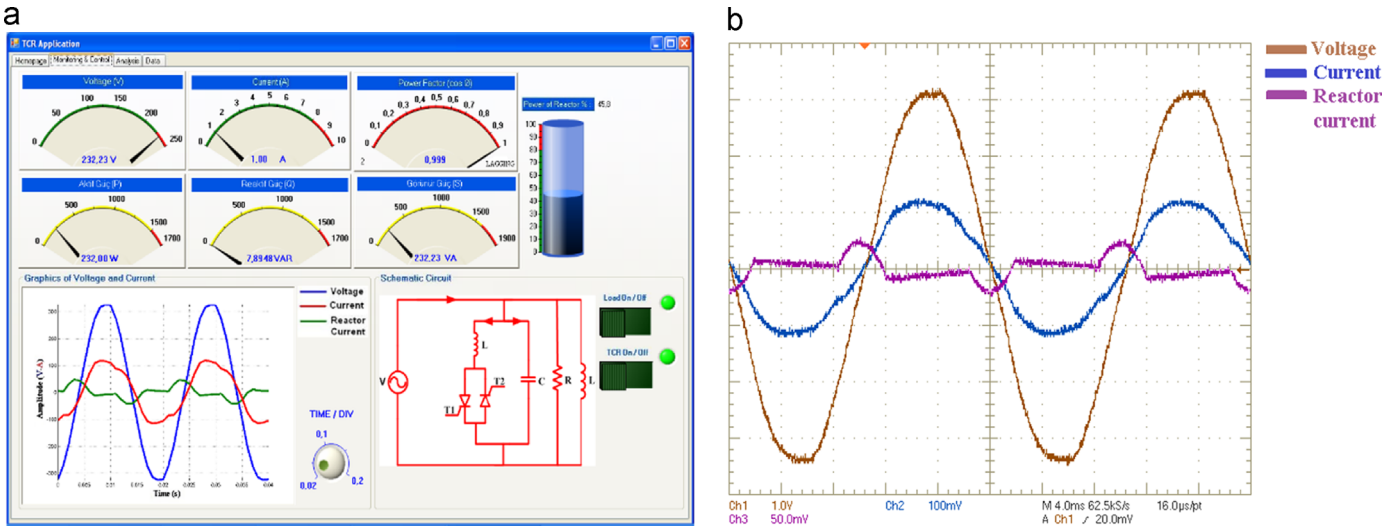

Fig. 15. (a) The view of interface after compensation ($R=257\ \Omega$, $L=0.85$ H, $C=14.02\ \mu$F). (b) Real time scope results for the same operational conditions.

is obviously seen that the electrical angle between the voltage and the current is decreased from 20 degrees to 1 degree and the power factor value is successfully improved to the 0.99 lagging.

Thanks to the system developed in this study, data measured in real time is not only monitored on the interface but also stored in a database automatically in each 100 ms. The recent data stored in

freepaper.me FREE paper

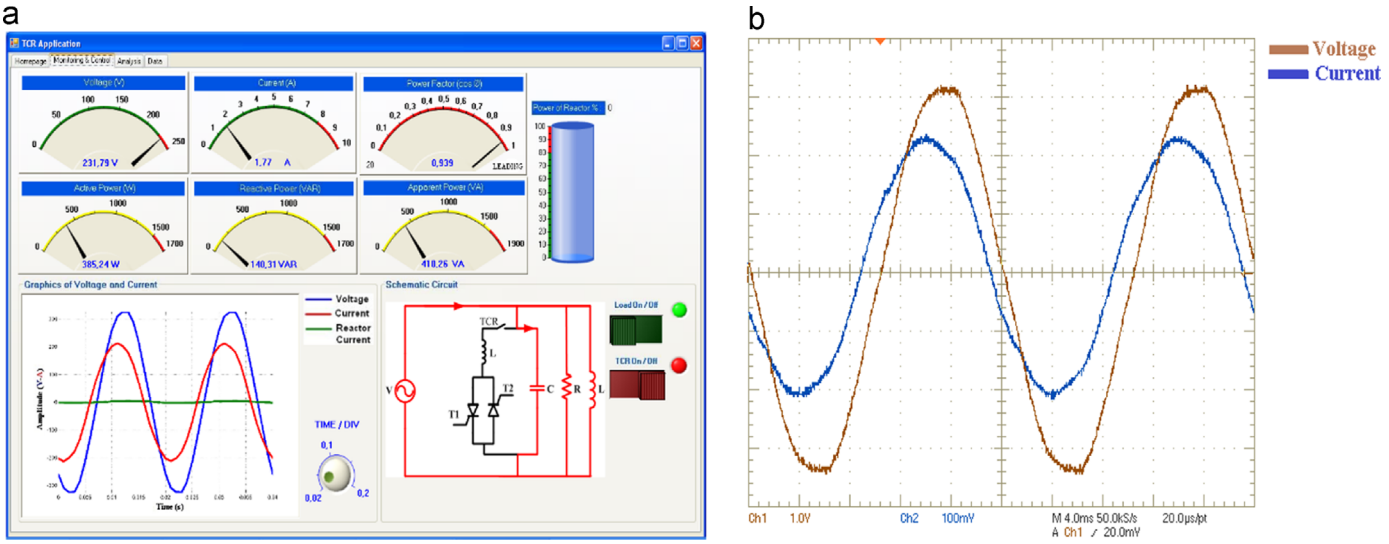

Fig. 16. (a) The view of interface before compensation ($R=139\ \Omega$, $L=1.78$ H, $C=14.02\ \mu$F). (b) Real time scope results for the same operational conditions.

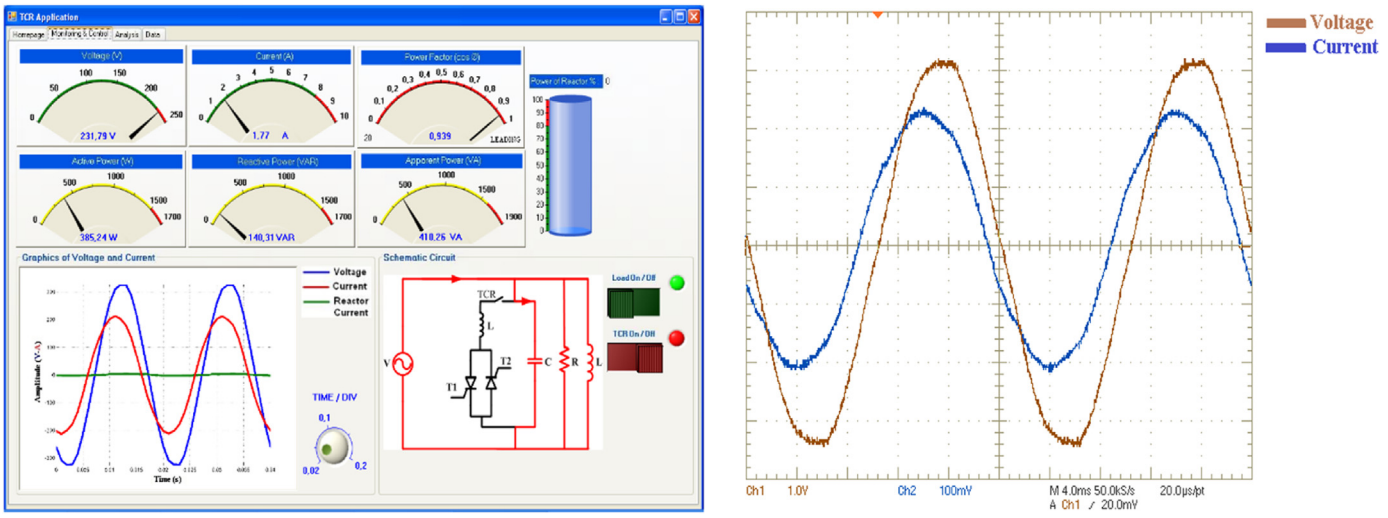

Fig. 17. (a) The view of interface after compensation ($R=139\ \Omega$, $L=1.78$ H, $C=14.02\ \mu$F). (b) Real time scope results for the same operational conditions.

database can be analyzed by filtering for a specific date range and current/voltage graphics can also be drawn through the interface as seen in Fig. 18.

5. Conclusion

This study aims to realize an advanced dynamic compensation system based on fixed capacitor thyristor controlled reactor (FC-TCR) and to design a visual interface for monitoring and controlling the system as computer aided. For this purpose, a simple power system model is designed and installed in laboratory conditions that includes real-time energy measurement units, microcontroller, loads, sensors, actuators, and so on. Instead of using commercial power analyzers, all necessary circuits are specially designed and integrated with a control unit to measure the system parameters, to calculate the power factor, to generate the PWM control signals and to drive the thyristors for compensation process. As the main controller, a dsPIC is used in the system because of its powerful features like efficiency, high speed, high resolution, low price, etc. Thus, it has been possible to trigger the thyristors accurately and measure the power factor quickly.

In addition to the compensation system, a visual interface is designed to monitor all system parameters graphically and numerically and also to perform the required operations easily through a control computer. A data acquisition board is used to transfer data and to manage communication processes between the computer and the other environmental hardware units employed in the system. All system parameters measured in real time can be also stored in a database to analyze them later if needed.

The system has been tested under several load conditions those have leaking and lagging power factors and it has been observed from the experimental results that the compensation system achieved in the study has considerably quick response time against the all operational conditions. Furthermore, the system immediately reacts the dynamic load variations and compensates to the power factor in a very short time. Although some current harmonics are generated because of using switching elements, fixed capacitors reduce them significantly. If needed, extra

freepaper.me FREE paper

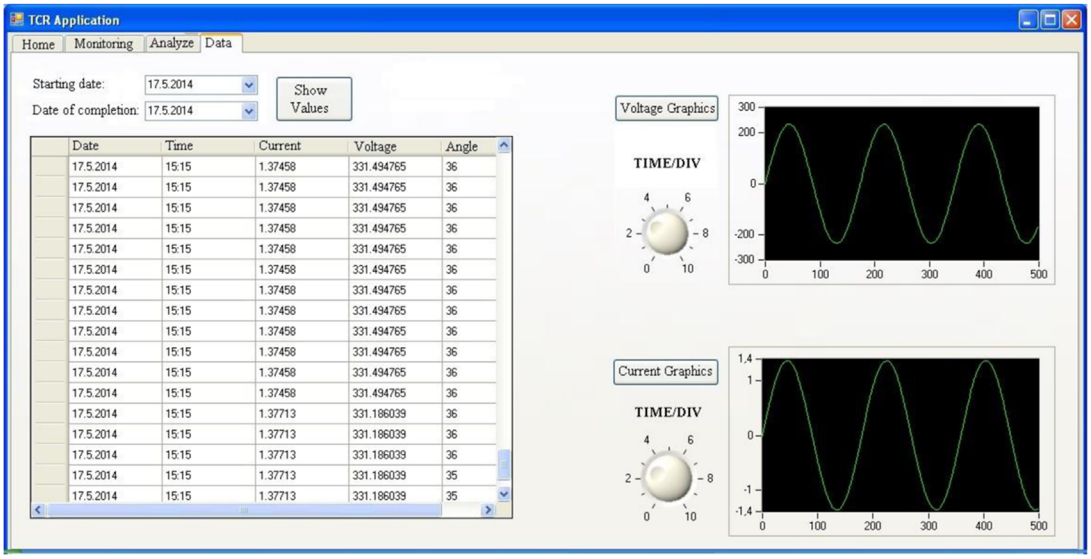

Fig. 18. Data storage screen of the interface.

harmonic filters can be added to the system easily to eliminate the harmonics.

The system presented will be a useful solution especially for the industrial plants, the reactive power demand of which continuously changes within a short time because of using high power and fluctuating nonlinear loads.

References

[1] Vardar T, Cam E, Yalcin E. Energy efficiency with reactive power compensation and reactive power compensation in public institutions. Int J Eng Res Dev 2010;2(2).

[2] The Republic of Turkey Energy Market Regulatory Authority, Regulation of electricity transmission system supply reliability and quality, Official Gazette of Turkish Republic, No: 27738; 2010.

[3] Bouafassa A, Rahmani L, Mekhilef S. Design and real time implementation of single phase boost power factor correction converter. ISA Trans 2015;55:267–74.

[4] Kara A, Yalcinoz T. Load compensation with open-close controlled FACTS devices. In: Proceedings of the 3th Automation Symposium; 2005. p. 68–72.

[5] Bayındır R, Kaplan O. Design of PIC controlled reactive power relay. J Fac Eng Archit Gazi Univ 2007;22(1):47–56.

[6] Shi C, Chen Y, Liu Z. Study of reactive power in AC/DC power system. In: Proceedings of the 2nd IEEE Conference on Industrial Electronics and Applications; 2007. p. 207–211.

[7] Rahmani S, Hamadi A, Al-Haddad K, Dessaint LA. A combination of shunt hybrid power filter and thyristor-controlled reactor for power quality. IEEE Trans Ind Electron 2014;61(5):2152–64.

[8] Colak I, Bayindir R, Bay OF. Reactive power compensation using a fuzzy logic controlled synchronous motor. Energy Convers Manag 2003;44:2189–204.

[9] Dixon J, Moran L, Radriguez J, Domke R. Reactive power compensation technologies, State of the art review. Proceed IEEE Publ 2005;93(12):2144–64.

[10] Lee SY, Wu CJ, Chang WN. A compact control algorithm for reactive power compensation and load balancing with static VAR compensator. Electr Power Syst Res 2001;58:63–70.

[11] Sannino A, Svensson J, Larsson T. Power-electronic solutions to power quality problems. Electr Power Syst Res 2003;66:71–82.

[12] Liu CW, Luo CC, Lin PY, Lu GC, Wu WC, Tsai JI et al. Developing a power quality measurement system integrated with HAN home energy management system. In: Proceedings of the 4th International Conference on Electric Utility Deregulation and Restructuring and Power Technologies; 2011. p. 1506–1510.

[13] Bayindir R, Kaplan O. Design and implementation of an internet based effective controlling and monitoring system with wireless fieldbus communications technologies for process automation-An experimental study. ISA Trans 2012;51:461–70.

[14] Montoya FG, Alcayde A, Sanchez P, Gomez J, Martin F. Energy: An open source project for power quality assessment and monitoring. In: Proceedings of the International Conference on Power Engineering Energy and Electrical Drives; 2011. p. 1–6.

[15] Le CV, Pang CK, Gan OP. Energy saving and monitoring technologies in manufacturing systems with industrial case studies. In: Proceedings of the 7th IEEE Conference on Industrial Electronics and Applications (ICIEA); 2012. p. 1916–1921.

[16] Dorhofer FJ, Heffington WM. Electrical energy monitoring in an industrial plant. In: Proceedings of the 16th National Industrial Energy Technology Conference, Houston; 1994.

[17] Yao WL, Ku CH. Developing a PC-based automated monitoring and control platform for electric power systems. Electr Power Syst Res 2003;64:129–36.

[18] Nagata T. An electric power energy monitoring system in campus using an internet. In: Proceedings of the IEEE Power Engineering Society General Meeting Canada; 2006. p. 1–6.

[19] Colak I, Bayindir R, Demirbas S, Bektas A. Observation of electric energy at an industrial plant. Inst Sci Technol J Erciyes Univ 2008;24(1–2):154–64.

[20] Figueiredo JM, Sada Costa JMG. An efficient system to monitor and control the energy production and consumption. In: Proceedings of the 5th International Conference on European Electricity Market; 2008. p. 1–6.

[21] Yingkayun K, Premrudeepreechacharn S. A power quality monitoring system for real-time detection of power fluctuations. In: Proceedings of the 40th North American Power Symposium (NAPS); 2008. p. 1–5.

[22] Irmak E, Calpbinici A, Guler N. Design of an energy monitoring system for a medium-scale plant. J Eng Sci Pamukkale Univ 2012;18(2):123–31.

[23] Cardenas A, Guzman C, Agbossou K. Real-time evaluation of power quality using FPGA based measurement system. In: Proceedings of the IEEE International Symposium on Industrial Electronics (ISIE); 2010. p. 2777–2782.

[24] Das S, Chatterjee D, Goswami SK. A gravitational search algorithm based static VAR compensator switching function optimization technique for minimum harmonic injection. Electr Power Components Syst 2015;43(20):2297–310.

[25] Padiyar KR. FACTS Controllers in power transmission and distribution. India: New Age International Publishers; 2007. p. 52–62.

[26] Hooshmand RA, Esfahani MT. Adaptive filter design based on the LMS algorithm for delay elimination in TCR/FC compensators. ISA Trans 2011;50:142–9.

[27] Mathur RM, Varma RK. Thyristor-based FACTS controllers for electrical transmission systems. USA: IEEE Press; 2002. p. 45–53.

[28] Irmak E, Colak I, Kaplan O, Guler N. Design and application of a novel zero-crossing detector circuit. In: Proceedings of the International Conference on Power Engineering, Energy and Electrical Drives, Malaga, Spain; 2011. p. 1–4.

freepaper.me FREE paper